Fuel 365 (2024) 131264

Contents lists available at ScienceDirect

Fuel

journal homepage: www.elsevier.com/locate/fuel

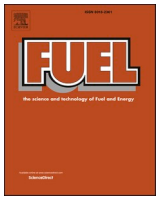

Full Length Article

Biomass-derived activated carbon catalysts for the direct dimethyl ether synthesis from syngas

José Palomo, Miguel Ángel Rodríguez-Cano, José Rodríguez-Mirasol *, Tomás Cordero

Universidad de Málaga, Andalucía Tech, Departamento de Ingeniería Química, 29010 Málaga, Spain

A B S T R A C T

The direct DME synthesis from syngas was studied by using activated carbon-based bifunctional catalytic beds. Two kinds of activated carbons, prepared by physical (by CO_2 partial gasification) and chemical (with phosphoric acid) activation of olive stones, were used as supports for the preparation of the catalysts. The chemically activated carbon presented a considerable amount of thermally and chemically stable surface phosphorus complexes, which played an important role on the catalytic performance of the prepared catalysts. A Zr-loaded P-containing activated carbon presented a relatively high activity, selectivity and stability for the production of DME from methanol and was used as methanol dehydration catalyst. On the other hand, Cu-Zn was loaded on both P-containing and P-free activated carbon supports for the preparation of methanol synthesis catalysts. The presence of surface-phosphorus on the carbon support resulted in a strong metal-support interaction, hindering the catalytic activity for the hydrogenation of CO to methanol. However, the catalyst that did not contain phosphorus showed noticeable activity for this reaction. The physical mixing of the methanol synthesis and methanol dehydration catalysts resulted in the preparation of carbon-based bifunctional catalytic beds, which performed very efficiently in the direct DME synthesis from syngas in a fixed-bed reactor. Different mass ratios of the individual (metallic and acid) catalysts were studied. An acid/metallic catalyst mass ratio of 2 provided the catalytic bed with enough acid sites to promote methanol dehydration to its maximum extent and make the overall product distribution controlled by the methanol synthesis reaction on the metallic phase.

1. Introduction

Dimethyl ether (DME) is a chemically stable, colorless, non-toxic, non-carcinogenic, and environmentally friendly compound presenting a characteristic odor. The physical and chemical properties, similar to liquified petroleum gases (LPG) [1] and conventional diesel [2,3], plus the clean combustion achieved when used as fuel [4], make this compound being considered as one of the most promising alternatives to petroleum derived fuels. Furthermore, DME can be used as intermediate for the production of chemicals and light olefins, and thus, its production is the object of much research [5–9].

DME can be produced by two alternative processes; a two-step catalytic process (so-called indirect process), which involves a first stage for methanol synthesis from syngas that takes place in parallel with the water gas shift reaction (WGSR) (Eq. (1), (2) and (4)) on Cu-based catalysts [10–12] and a second stage for the selective dehydration of methanol to DME (Eq. (3)) on a solid acid catalyst [13–16]; and a one-step process (so-called direct process), in which synthesis gas is fed to a single reactor containing a bifunctional catalyst, where both methanol synthesis, in parallel with the WGSR, and the selective methanol dehydration to DME take place [17–23].

$$2CO + 4H_2 \leftrightarrow 2CH_3OH \ (\Delta H_r^\circ = -90.8 \ kJ{\cdot}mol^{-1}) \quad (1)$$

$$CO_2 + 3H_2 \leftrightarrow CH_3OH + H_2O \ (\Delta H_r^\circ = -49.5 \ kJ{\cdot}mol^{-1}) \quad (2)$$

$$2CH_3OH \leftrightarrow CH_3OCH_3 + H_2O \ (\Delta H_r^\circ = -21.3 \ kJ{\cdot}mol^{-1}) \quad (3)$$

$$H_2O + CO \leftrightarrow H_2 + CO_2 \ (\Delta H_r^\circ = -41.1 \ kJ{\cdot}mol^{-1}) \quad (4)$$

Although the industrial DME production is currently carried out by the indirect process, the prospects for the development of a DME-based economy depends on the feasibility of the direct DME synthesis route [24]. The main motivation for using the direct route instead of the conventional indirect one relies on the thermodynamic limitations affecting the latter. Chemical reactions involved in methanol synthesis are reversible and they are limited by thermodynamic equilibrium, which is a function of the temperature, pressure and the synthesis gas composition. This thermodynamic limitation results in a low synthesis gas conversion per-pass, increasing the operating costs related to methanol separation and synthesis gas recirculation [25]. The use of the direct DME synthesis route, allows for in-situ consuming the generated methanol, via dehydration to DME, reducing the equilibrium constrains affecting the methanol synthesis in this way. This thermodynamic advantage lets working at lower pressure and/or higher temperature achieving a higher synthesis gas conversion per pass [19,26]. On the other hand, the water generated in the methanol dehydration reaction

* Corresponding autor.
E-mail address: mirasol@uma.es (J. Rodríguez-Mirasol).

https://doi.org/10.1016/j.fuel.2024.131264
Received 2 December 2023; Received in revised form 7 February 2024; Accepted 20 February 2024
Available online 27 February 2024

(Eq. (3)), can be removed from the reaction media by means of the WGSR (Eq. (4)), yielding H_2 and favoring the methanol dehydration reaction. This feature is of high interest when using a CO-enriched synthesis gas, which present a low hydrogen concentration, such as that obtained via biomass gasification [27–31]. In this sense, the use of biomass derived synthesis gas for this process would lead to a considerable reduction of greenhouse gasses emissions in this process, promoting the transition to an energy system that reduces dependence on fossil fuels in a scenario that contemplates, on the one hand, the scarcity of fossil fuels and, on the other hand, the growth of global demand and the impact of emissions on the environment [32]. Another approach is the use of CO_2 instead of CO via direct hydrogenation of CO_2-to-DME (CTD) [33], which is receiving much attention as an strategy for recycling CO_2 and using DME as circular hydrogen carrier [34–36].

The catalysts used for the direct DME synthesis route are composed of two active phases, one accounting for the methanol synthesis and another one for the methanol dehydration. As a component for methanol synthesis, the most commonly used catalytic phase is the $Cu/ZnO/Al_2O_3$ ternary system [10]. Recently the system $Cu/ZnO/ZrO_2$ [6,37] is also taking importance. The acid component involved in these catalysts must present a moderate acid strength, being enough so as to promote methanol dehydration, but not too high, so as to avoid further DME dehydration to olefins and higher hydrocarbons (which are related to coke formation). The most commonly studied acid functions for bifunctional catalysts are γ-Al_2O_3 [38,39], HZSM-5 [20,40,41], HMCM-22 [42], ferrierite [43,44], mordenite [45] and SAPOs [24].

In the last decades, activated carbons have been widely investigated as catalysts and catalyst supports. These materials present remarkable features, such as high thermal and chemical stability, and high specific surface area. Moreover, they can be obtained from several kinds of lignocellulosic waste [46,47], giving rise to economic advantages. Despite the potential they have exhibited, to the best of our knowledge, the use of activated carbon-based catalysts for the direct DME synthesis has not been reported to date. Only a very limited number of studies targeting the individual reaction steps, namely: synthesis of methanol using carbon based support [48–51] and the application of activated carbons for the methanol dehydration reaction [52–54] can be found in the literature. On the other hand, whereas the preparation of catalysts reasonable active and stable for the methanol synthesis have shown a higher degree of success, achieving an active and stable methanol dehydration catalyst has presented more difficulties. In this sense, the carbon-based catalysts reported in the literature dealing with methanol dehydration presented acid groups with very low thermal stability, which resulted in a fast deactivation of the catalysts at the reaction temperatures, making them not suitable as acid component for the direct DME synthesis operation conditions. On the other hand, the preparation of activated carbons by chemical activation with phosphoric acid under specific conditions yields carbons materials containing high thermal and chemically stable oxygen-phosphorus acid surface groups [55–57]. The use of these activated carbons for the methanol dehydration reaction showed that, although these materials performed very efficiently under air atmosphere, achieving a selectivity to DME higher than 90 % with a DME yield of 40 % at 350 °C, they were fast deactivated under a non-oxidizing atmosphere [58], and thus, their application as acid component of bifunctional catalytic systems for the direct DME synthesis was not feasible neither.

More recently, we reported that the modification of phosphorus-containing activated carbons with zirconium yields carbon materials presenting zirconium phosphate species, which presented a remarkable efficiency in the selective methanol dehydration to DME reaction under non-oxidizing atmosphere [59]. In this sense, high steady-state methanol conversion values, keeping a selectivity to DME higher than 97 %, were obtained in the whole range of temperatures studied (250–400 °C) [60], which lays in the range of operation temperature for the direct DME synthesis, resulting in DME yields up to 80 %. After this breakthrough, other combinations of transition metals-carbon functional groups, such as W-O-P were explored [61,62], further confirming the high stability of carbon based materials presenting P and transition metals as active sites for promoting the selective methanol dehydration to DME. Therefore, these activated carbon catalysts could be feasibly used as the methanol dehydration component in the direct DME synthesis from syngas.

In this work, we explore the direct synthesis of DME using biomass waste-derived bifunctional catalytic beds that, to the best of our knowledge, has not been reported to date. As for methanol synthesis component, different activated carbons were loaded with Cu/Zn, and the effect of surface chemistry, especially the presence of heteroatoms on the carbon surface, on the catalytic performance of the methanol and DME synthesis is thoroughly analyzed. The use of the biomass waste-derived catalysts presented here could be also beneficial from the environmental and economical point of view. On the one hand, it is worth to mention that the catalysts were prepared from an inexpensive agri-food industrial waste. Moreover, in the event of these catalyst being irreversibly deactivated, they can be further valorized via combustion, making energy recovery possible, or via partial gasification with CO_2 (from carbon capture and storage) or water vapor, generating valuable syngas; with both approaches providing an inorganic residue (ashes) containing the metal phases. In this way, circularity of the Syngas-to-DME can be enhanced, reducing the carbon footprint of the process.

2. Experimental method

2.1. Preparation of the activated carbon supports

Two kinds of activated carbons were prepared. On the one hand, an activated carbon was prepared by physical activation. For this process, 15 g of olive stone, an agri-food industry residue, was carbonized and then it was partially gasified with CO_2. Both stages were carried out in a conventional tubular laboratory furnace. In the carbonization step, the sample was heated at 10 °C/min up to 800 °C, keeping this temperature for 2 h, under continuous N_2 flow (150 cm^3/min STP). Afterwards, the carbonized sample was partially gasified using a continuous CO_2 flow (150 cm^3/min STP) at the same temperature for 7 h, obtaining a 42 % burn-off. The final carbon presented a mass yield of 14 % based on the mass of dried olive stone. Finally, this sample was grinded and sieved (100–300 μm) and was denoted as *ACG*. On the other hand, an activated carbon was prepared via chemical activation of olive stones, with phosphoric acid. For the activation process, 10 g of olive stone was impregnated with H_3PO_4 85 %(w/w) aqueous solution, at room temperature and dried for 24 h at 60 °C. An impregnation ratio (H_3PO_4/olive stone mass ratio) value of 2 was used in this work. Once dried, the impregnated substrate was activated in a conventional tubular furnace under continuous N_2 flow (150 cm^3/min STP) at 800 °C for 2 h. The activated sample was cooled down to room temperature inside the tubular furnace, keeping the same N_2 flow and afterwards it was washed with distilled water at 60 °C, until achieving a neutral pH and a negative phosphate analysis in the eluate [55]. The activated carbon presented a final mass yield of 39 % based on the mass of dried olive stone and was denoted as *ACP*. Finally, activated carbon was grinded and sieved (100–300 μm).

2.2. Catalysts preparation

The activated carbons were loaded with Cu, Zn and Zr salts to prepare the carbon-based catalysts used in this work. Fig. 1 shows an outline of the procedures and nomenclature used for the preparation of the catalysts.

2.2.1. Methanol dehydration catalyst preparation. Zr loading

Zr loading was carried out by incipient wetness impregnation at room temperature. A 5 %(w/w) of zirconium was loaded on the activated carbon obtained by chemical activation, *ACP*, using a $ZrO(NO_3)_2$

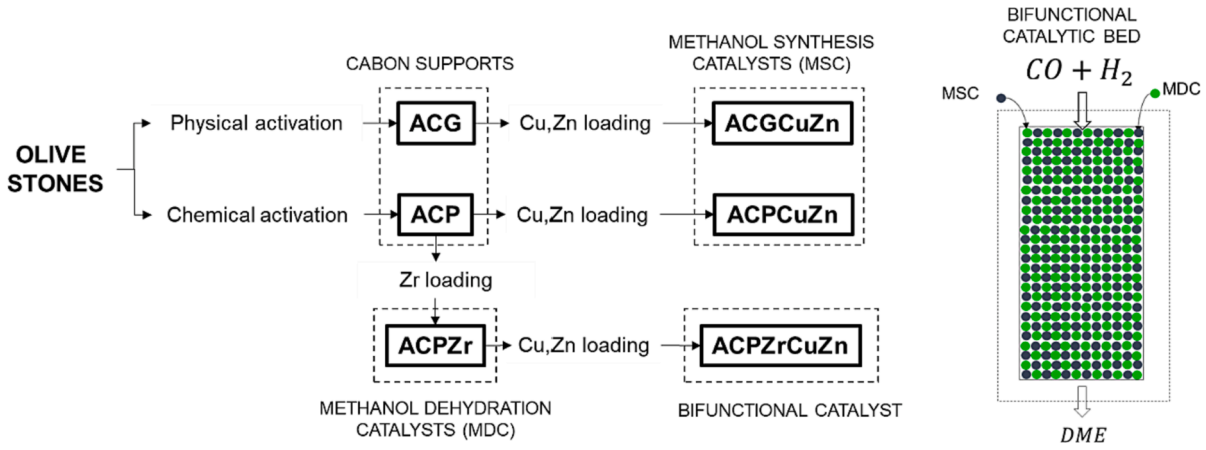

Fig. 1. Schematic diagram of the procedures and nomenclature used for sample preparation of the catalysts and the bifunctional catalytic beds.

in water solution. For the impregnation step, batches of about 1 g was used. Once impregnated, the sample was dried overnight at 120 °C and then calcined at 250 °C (heating rate of 10 °C/min) for 2 h in a tubular furnace under continuous air flow (150 cm^3/min STP). This sample was denoted as *ACPZr*.

2.2.2. Methanol synthesis catalysts preparation. Cu-Zn loading

Cu-Zn loading was carried out on the two different activated carbons, *ACG* and *ACP*. In addition, the use of the methanol dehydration catalyst, *ACPZr*, as support for the Cu-Zn metallic phase was addressed. The metal loading process was carried out at room temperature by pore-volume impregnation of the previously dried samples at 120 °C. In this process, an appropriate amount of $Cu(NO_3)_2{\cdot}3H_2O$ and $Zn(NO_3)_2{\cdot}6H_2O$ was previously dissolved in the distilled water and added to a known quantity of activated carbon to prepare catalysts with a Cu and Zn loading of 10.5 and 5.5 %(w/w), respectively. The impregnated carbons were dried at 120 °C for 24 h and finally calcined at 300 °C for 4 h under continuous N_2 flow (150 cm^3/min STP). The catalyst obtained were denoted by adding *CuZn* to the name of the parent carbon.

2.2.3. Bifunctional catalytic beds preparation

The preparation of bifunctional catalytic beds was carried out by physical mixing of the corresponding methanol synthesis and methanol dehydration components, by using different acid/metallic mass ratios. Physical mixtures were denoted as *Metallic component name* + *X Acid component name*, being *X* the Acid/metallic mass ratio.

2.3. Characterization of the carbon catalysts

The porous texture of the activated carbons and catalysts was characterized by N_2 adsorption–desorption at −196 °C and by CO_2 adsorption at 0 °C, performed in an ASAP 2020 equipment (Micromeritics). Samples were previously outgassed for 8 h at 150 °C. From the N_2 adsorption–desorption isotherm, the apparent surface area (A_{BET}) was determined applying the BET equation [63], the micropore volume (V_t ^{N2}) and the external surface area were calculated using the t-method [64] and the mesopore volume (V_{mes}^{N2}) was determined as the difference between the adsorbed volume at a relative pressure of 0.96 and the micropore volume of V_t ^{N2}. The narrow micropore volume (V_{DR} ^{CO2}) and surface area (A_{DR} ^{CO2}) were calculated by the Dubinin–Radushkevich equation [65], applied to the CO_2 adsorption isotherm.

The surface chemistry of the samples was analyzed by X-ray photoelectron spectroscopy (XPS). XPS analyses of the samples were obtained using a VersaProbe II ESCA 5701 model Physical Electronics apparatus, with Al Kα radiation (1486.6 eV). For the analysis of the XPS peaks, the C1s peak position was set at 284.5 eV and used as reference for the other peaks [66,67].

The reducibility of the Cu species present on the catalysts was studied by temperature programmed reduction (H_2-TPR). For these analyses, 50 mg of dried sample was loaded in a quartz fixed-bed reactor and were heated up to 100 °C under helium flow. Then the helium flow was switched to a 10 %(v/v) H_2 in helium stream, and kept for 30 min. Finally, the sample was heated up to 350 °C at a heating rate of 5 °C/min. H_2 consumption was monitored by mass spectrometry (Pfeiffer Omnistar GCD-301), registering the signal *m/z* 2.

The total acidity and acid strength distribution of the methanol dehydration catalyst was determined by temperature programmed desorption of ammonia (NH_3-TPD). In these analyses 100 mg of dried sample was heated up to 100 °C under helium flow and then it was saturated with NH_3 (20 %(v/v) in helium) for 15 min at the same temperature. Afterwards, the weakly adsorbed NH_3 was desorbed in continuous helium flow at 100 °C until no NH_3 was detected in the outlet stream. The NH_3-TPD experiment was carried out by rising the temperature up to 500 °C at a heating rate of 10 °C/min. The outlet NH_3 concentration was registered using a TCD-detector and by mass spectrometry.

2.4. Catalytic experiments

The catalytic experiments for the direct DME synthesis from synthesis gas were carried out in a PID Eng. & Tech. Microactivity equipment, which is provided with a stainless steel fixed-bed reactor (i.d. 9 mm) and allows for operating at high temperature and pressures. Prior to stating the reaction, the catalyst was in-situ reduced at 270 °C under H_2 flow (50 mL/min) for 2 h. After the reduction step, the temperature was set to the reaction value, and afterwards, the pressure was slowly increased up to the desired value. Finally, the synthesis gas was introduced. To prevent the condensation of any compound, all lines were heated up to 120 °C. The outlet gas concentrations were analyzed by online gas chromatography (Perkin-Elmer Clarus 500 GC equipped with TCD and FID detectors). The used columns were a Permanent gases active carbon 80/100 mesh for CO and CO_2 analysis and a 1.9 m x 1/8″ x 2.1 mm Porapak N 80/100 + 0.5 m x 1/8″ x 2.1 mm Porapak Q 80/100 column for methanol, DME and light hydrocarbons separation. N_2 was used as internal standard for GC analyses.

The conversion was defined as the ratio of the amount of reacted CO to that of supplied CO to the reactor. The selectivity (in %mol) was defined as the ratio of carbon moles in a specific product referred to the moles of converted CO into all the products formed. The yield to DME was calculated as the product of the CO conversion and the selectivity to DME.

3. Results and discussion

3.1. Characterization of the carbon catalysts

Fig. 2 shows the N_2 adsorption–desorption isotherms at −196 °C of the different activated carbon materials prepared in this study. Physically activated carbon, ACG, presented a type I a isotherm [68], adsorbing almost all N_2 volume at low relative pressures, which is characteristic of a predominantly microporous texture. Chemically activated carbon, *ACP*, showed a type I b isotherm, associated to the presence of a broad range of wider micropores and narrow mesopores. The existence of a H4 type hysteresis loop is noticeable, closing at a relative pressure value of 0.4, indicative of capillary condensation in mesopores [68].

After any metal deposition, both activated carbons presented a reduction in their porous texture. The methanol dehydration catalyst, *ACPZr*, showed a slight decrease in the volume of N_2 adsorbed in the range of the low relative pressures, as compared to the parent carbon, *ACP*, indicating a reduction of the wider microporosity, due to Zr loading. Cu-Zn loading resulted in a more noticeable porosity reduction, due to the higher amount of metal loaded on the carbon supports. In this sense, the three samples used as Cu-Zn support, *ACG*, *ACP* and *ACPZr*, showed a reduction in the volume of N_2 adsorbed, but in this case at a very low relative pressures, which indicates a narrow micropore reduction or blockage.

Table 1 shows the textural parameters obtained from N_2 adsorption–desorption and CO_2 adsorption isotherms. Both activated carbons presented a well-developed porous texture and high surface areas. Physically activated carbon, ACG, presented an A_{BET} value similar to A_{DR}, indicating a microporous texture. The similarity between V_t and V_{DR} further confirmed the presence of a narrow microporous texture. The chemically activated carbon, *ACP*, presented a comparable A_{BET} value to that obtained for the physically activated carbon, *ACG*. However, attending to the higher value of A_{BET} as compared to A_{DR}, this sample presented a wider microporous texture, as compared to the physically activated carbon. Moreover, the high mesopore volume value (V_{mes}) when comparing with the micropore volume one (V_t), together with the high external surface area value (A_t), suggested a high contribution to mesoporosity in this material.

Once metals were loaded on the support, both activated carbons showed a decrease in the textural parameters as compared to the parent activated carbon. The Zr loaded chemically activated carbon showed a slight decrease, in general, in the textural parameters when compared to the ones of the parent activated carbon, suggesting that Zr was homogeneously distributed both on the external and internal surface of the activated carbon particles. After Cu-Zn loading a more significant decrease in the textural parameters was observed in all the samples. In these cases, A_{BET} and A_{DR} decreased in a similar way, indicating a reduction in the microporosity of these samples. The decrease in the V_t and V_{DR} values suggested the blockage of the narrow micropores due to metal deposition.

X-ray photoelectronic spectroscopy (XPS) analyses were carried out to evaluate the surface chemical composition of the carbons. Table 2 reports the atomic surface composition of the samples. Both activated carbon supports, *ACG* and *ACP*, were mainly composed by carbon (91.7 and 89.7 % (w/w), respectively) and oxygen (7.3 and 7.2 % (w/w), respectively). In addition, the chemically activated carbon, *ACP*, presented a considerable amount of phosphorus (3.1 % (w/w)), presumably in form of phosphate groups [55]. The presence of phosphorus has been attributed to the activation step with phosphoric acid [57], which is reported to proceed through the formation of phosphate and polyphosphate bridges that connect and crosslink biopolymer fragments [69]. As a result of this activation mechanism, part of these phosphorus complexes remain chemically bonded to the carbon surface, even after the washing step [70].

After Zr loading on the chemically activated carbon, *ACP*, an increase in both Zr and O was observed. Attending to the surface composition, a higher amount of O, when compared to the maximum theoretically introduced if Zr were deposited on the carbon surface in form of ZrO_2, was observed (see *ACPZr* in Table 2). This fact could be associated to the surface oxidation of these activated carbon catalysts during the thermal stabilization process (calcination) at 250 °C [55]. As expected, the three Cu-Zn containing catalysts exhibited the presence of these elements, Cu and Zn, on their surface. In addition, as occurred when loading with zirconium, the oxygen content increased to a higher extent than that expected considering the incorporation of Cu and Zn as oxides (CuO and ZnO). In this case, the increase in the oxygen content could be related to the metal salts decomposition during thermal treatment, which has been reported to yield oxygen groups on the activated carbon surface [71].

In order to analyze in depth the surface chemistry of the activated carbon catalysts, the XPS spectra were examined. Fig. 3 shows the normalized high resolution multiregional XPS spectra for phosphorus, zirconium and copper. The P2p spectrum of the chemically activated carbon, *ACP*, showed a main peak at 133.2 eV, associated to the presence of pentavalent tetracoordinated phosphorus, presumably forming C-O-PO_3 and C- PO_3/C_2-PO_2 surface groups bonded to the carbon surface [70,72]. After Zr loading, the P2p spectrum for *ACPZr* shifted to higher binding energy values (133.7 eV), indicating the oxidation the phosphorus surface groups, which probably occurred during the calcination stage at 250 °C (see *ACPZr* in Fig. 3a) [55]. Cu-Zn loading process did not affect the P2p spectra of the samples in a significant extent. The normalized Zr3d spectra the two Zr-containing carbons, *ACPZr* and *ACPZrCuZn*, exhibited the two 3d peaks separated by 2.3 eV, characteristic of the of the tetravalent Zr^{4+}. The binding energy at which the $Zr3d_{5/2}$ appeared (183.1 eV), in both cases, was very similar to that reported for when analyzing zirconium phosphates [73,74], indicating

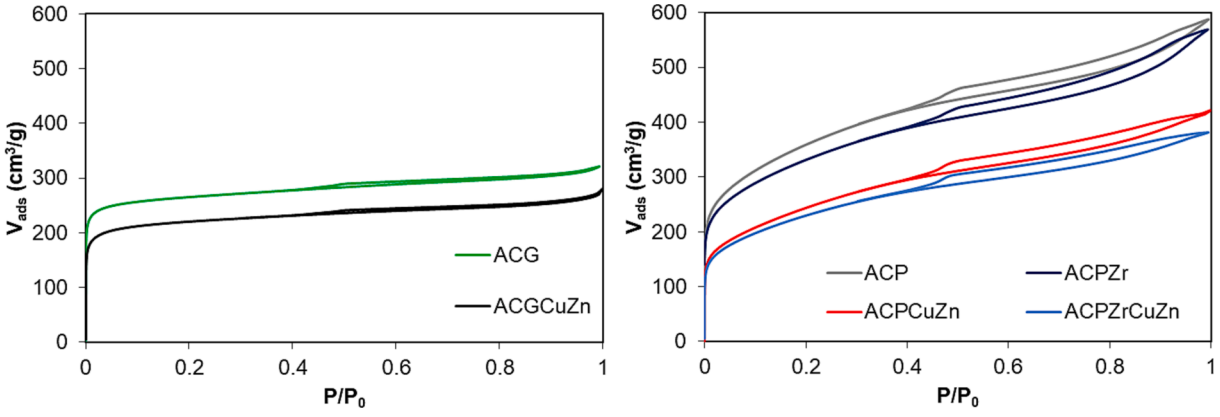

Fig. 2. Nitrogen adsorption–desorption isotherms at − 196 ∘C of the carbon materials.

Table 1
Characteristic parameters of the porous texture for the prepared carbon-based materials.

	N_2 Isotherm					CO_2 Isotherm	
	A_{BET}	V_p	V_{mes}	A_t	V_t	A_{DR}	V_{DR}
	(m^2/g)	(cm^3/g)	(cm^3/g)	(m^2/g)	(cm^3/g)	(m^2/g)	(cm^3/g)
ACG	1040	0.49	0.11	89	0.38	855	0.34
ACGCuZn	750	0.43	0.11	87	0.31	595	0.24
ACP	1260	0.9	0.42	295	0.49	470	0.19
ACPZr	1190	0.88	0.42	270	0.46	500	0.20
ACPCuZn	880	0.65	0.30	210	0.35	445	0.18
ACPZrCuZn	830	0.59	0.27	200	0.32	375	0.15

Table 2
Mass surface concentration values obtained by XPS.

Catalyst	Mass surface concentration (%)					
	C	O	Cu	Zn	P	Zr
ACG	91.7	7.3	–	–	–	–
ACGCuZn	50.4	17.3	25.5	6.8	–	–
ACP	89.7	7.2	–	–	3.1	–
ACPZr	59.8	19.6	–	–	5.7	14.9
ACPCuZn	36.6	23.3	24.3	11.3	4.5	–
ACPZrCuZn	36.4	26.6	13.5	7.1	4.4	12.1

the coordination of Zr atoms with a high number of strongly polarized oxygen atoms, forming P-O-Zr bonds, and thus suggesting the presence of zirconium phosphate species bonded to the activated carbon surface [59].

The normalized Cu2p$_{3/2}$ XPS spectra of the catalysts showed appreciable differences, which could be associated to the surface chemistry of the activated carbon support. On the one hand, the catalyst prepared by using the physically activated carbon as support, *ACGCuZn*, showed a binding energy value of 933.8 e.V. for the Cu2p$_{3/2}$ peak, and the presence of the strong satellite peaks between 940 and 945 eV, which are characteristic of Cu^{2+} in form of CuO [75,76]. On the other hand, when analyzing the catalyst prepared by using the chemically activated carbon as support, *ACPCuZn*, it could be seen that the Cu2p$_{3/2}$ peak showed a doublet structure and a significant decrease of the satellite peaks between 940 and 945 eV, which suggested the co-existence of non-reduced and reduced copper species. Similar observations have been reported when analyzing copper phosphate glasses [77,78]. These studies claimed that some of the Cu^{2+} was reduced to Cu^{+} upon going from CuO to Cu phosphate, being this doublet structure in the Cu2p$_{3/2}$ peak associated to the presence of both Cu^{+} (932.5 eV) and Cu^{2+} (934 eV) in the copper phosphate glass [78]. Given that the chemically activated carbon used as support in this study showed the presence of phosphorus, in form of phosphate groups, chemically bonded to its surface, the results here obtained suggested that Cu was interacting with P, forming copper phosphate species. *ACPZrCuZn*, also containing phosphorus, showed the same doublet structure for the Cu2p$_{3/2}$ peak. The Cu2p$_{3/2}$ peak of the phosphorus-containing samples was deconvoluted into two different peaks, associated to Cu^{+} and Cu^{2+}, at binding energies of 932.5 and 934 eV, respectively. The results showed that 65 % of the total Cu was in form of Cu^{+} in the sample *ACPCuZn*, whereas a value of 45 % was obtained for *ACPZrCuZn*. This difference could be justified given that the presence of Zr forming zirconium phosphate species on the sample *ACPZrCuZn* partially hindered the formation of copper phosphate species, remaining a higher amount of the Cu as CuO.

The reducibility of the Cu species present on the activated carbon catalysts was studied by temperature programmed reduction (H_2-TPR). Fig. 4 shows the H_2 consumption as a function of the temperature during H_2-TPR analysis for the metal-loaded activated carbons. The reduction of ZnO and ZrO_2 does not occur in a significant extent under the TPR

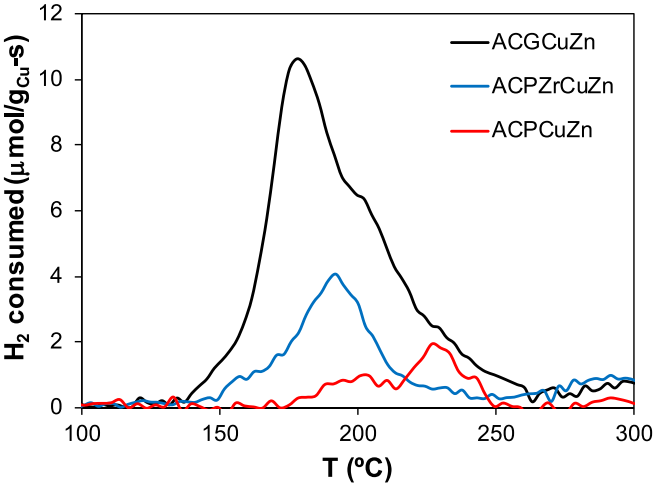

Fig. 4. H_2-TPR profile of Cu-Zn loaded activated carbon catalysts.

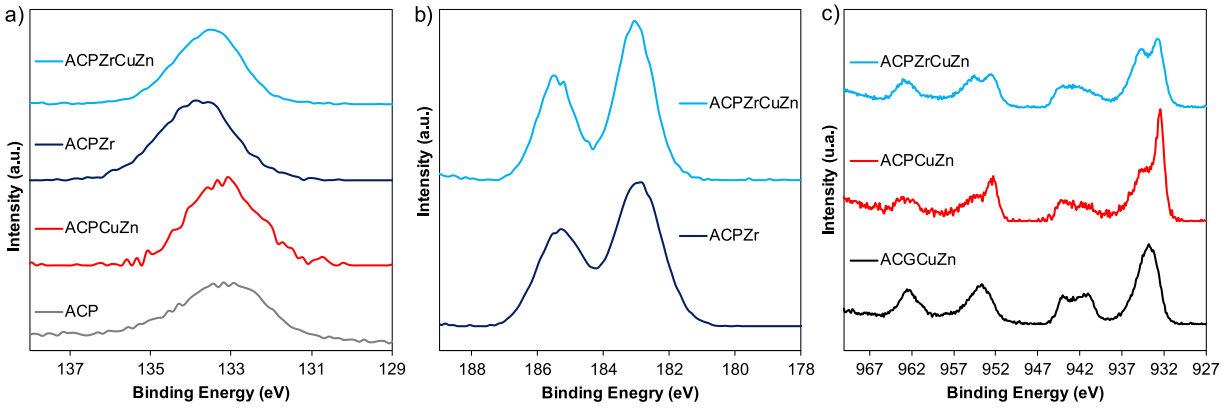

Fig. 3. Normalized XPS spectra for the prepared activated carbon samples. **a)** P2p, **b)** Zr3d and **c)** Cu2p.

conditions region analyzed [37]. On the other hand, the gasification of the activated carbon support has been reported to be very low, only being observed small amounts of methane at temperatures above 300 °C [48]. Therefore, the H_2 consumption measured during H_2-TPR was related to the reduction of the Cu species. *ACGCuZn*, presented a main H_2 consumption peak at about 180 °C, which was associated to the reduction of highly dispersed CuO [37] and a second at about 210 °C, related to bulk CuO reduction [79]. H_2-TPR deconvolution indicated that highly dispersed copper species accounted for 63 % of the total H_2 consumption species, whereas remaining 37 % was corresponding to bulk CuO reduction. The temperature at which the reduction of the CuO species occur depends on their particle size (the bigger particle size, the higher reduction temperature) [28] and also on the interaction between Cu and the other compounds present in the material [80,81]. The CuO reduction temperature for this catalyst was considerably lower than that reported for CuO-ZnO-Al_2O_3-based catalysts (about 300 °C) [17,82,83]. This fact is attributed to the weak interaction CuO-activated carbon as compared to other oxidic supports [48]. The phosphorus-containing samples, *ACPCuZn* and *ACPZrCuZn* showed a much lower H_2 consumption as compared to the sample prepared by using the physically activated carbon (not containing P) as support. Along this line, *ACPCuZn*, showed a negligible H_2 consumption, indicating the lack of reducibility of the Cu species present on this catalyst, with only a small H_2 consumption peak at a temperature 230 °C. *ACPZrCuZn*, showed a slightly higher H_2-consumption, as compared to *ACPCuZn*. The H_2 consumption profile showed one broad peak, centered at a temperature of 190 C. H_2-TPR deconvolution was carried out in the same way as in the *ACGCuZn* sample, being obtained that, in this case, 52 % of the total H_2 consumption was associated with the reduction of highly dispersed Cu species. Cu reducibility in the studied samples was also quantified by integrating the H_2-TPR profiles. The results showed a very low extent of reduction for the Cu species in the case of *ACPCuZn* sample, with just a 4 % of the Cu reduced upon H_2-TPR. This can be attributed to the strong interaction between Cu and P species present on the surface of this catalyst, in the form of Cu phosphate, which hinders Cu reduction. In the case of introducing Zr prior to the further Cu-Zn loading, *ACPZrCuZn* catalyst, the Cu extent of reduction significantly increased, reaching a value of 20 %. This is in line XPS findings which evidenced a lower amount of Cu phosphate species in the sample, due to the interaction of Zr and P forming zirconium phosphate species taking place prior to Cu-Zn loading. In the case of the catalyst not containing P on its surface, *ACGCuZn*, the Cu extent of reduction calculations evidenced that 48 % of the Cu is reducible under H_2-TPR conditions and thus accessible on the surface of the activated carbon support. The results shown above indicate that only CuO species were reduced, whereas Cu phosphate species present on the activated carbon surface were not reducible under H_2-TPR conditions.

Fig. 5 presents the NH_3-TPD profile obtained for the methanol dehydration catalysts used in this study, *ACPZr*. The temperature at which ammonia desorption occurs depends on the strength of the acid sites present on the materials, being the weaker centers the ones in which ammonia desorption occurs at the lower temperature. The acid strength required for efficiently dehydrating methanol to DME must be enough so as to promote methanol dehydration, but not too high, so as to avoid further DME dehydration to olefins and higher hydrocarbons (which are related to coke formation) [84]. The acid catalyst here presented desorbed most of the ammonia at a temperature lower than 300 °C, which highlighted the existence of acid sites presenting a weak/moderate strength. In this line, this weak/moderate acid character, related to the presence of Zr-O-P groups on the carbon surface, conferred the catalyst a suitable acidity for the selective methanol dehydration to DME [59,60].

3.2. Catalytic experiments

The Cu-Zn-containing carbon catalysts, *ACGCuZn*, *ACPCuZn*, and *ACPZrCuZn*, were first analyzed in order to stablish the most suitable methanol synthesis catalyst for the preparation of the bifunctional catalytic beds. Fig. 6 shows the CO conversion and selectivity to the main reaction products as a function of the temperature for the carbon catalysts (T = 250 – 300 °C, GHSV = 36.4 $L \cdot g_{Cu}^{-1} \cdot s^{-1}$, P = 45 bar, H_2/CO = 3). *ACGCuZn* showed noticeable CO conversion values in the temperature range studied. Attending to the selectivity to the main reaction products, it can be observed that a high selectivity to methanol (S_{MeOH} = 82 %) was obtained at 250 °C, which decreased when rising the temperature due to the formation of DME and CO_2, via methanol dehydration and water gas shift reaction, respectively. The dehydration capability of this catalyst under syngas to DME conditions was surprising, given that the parent activated carbon support, ACG, has been reported to be not active for methanol dehydration [59,60] and Cu-based catalysts have been also reported to form methanol through CO hydrogenation with a very high selectivity [85,86]. Therefore, the methanol dehydration capability of this material must be related to the presence of oxygen surface groups bonded to the carbon surface, which could have been generated during the metal salts decomposition thermal treatment [71] and also during CuO carboreduction. In this sense, temperature programmed decomposition analyses (TPD) performed over this sample indicated the presence of oxygen surface species that decompose yielding CO_2 during this thermal treatment (see Figure S1), suggesting the presence of surface oxygenated groups with surface acidity. *ACPCuZn*, showed very low CO conversion values, which can be justified based on the lack of reducibility of the Cu species presented on the surface of this catalyst (See Fig. 4). *ACPZrCuZn*, showed a higher CO conversion value, as compared to the other phosphorus-containing sample, *ACPCuZn*, due to the higher proportion of reducible Cu species in the former. Regarding the selectivity to the main reaction products, it could be observed that this sample presented the highest dehydration activity amongst the prepared catalysts, due to the presence of zirconium phosphate surface groups on the carbon surface, which are capable of promoting the selective methanol dehydration to DME [59,60].

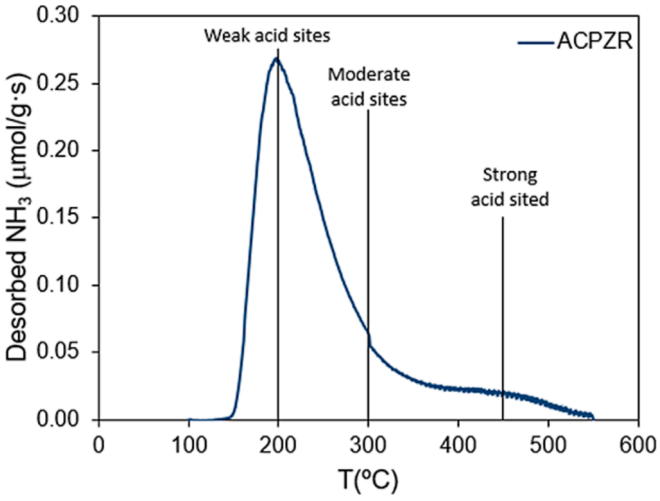

Fig. 5. Ammonia TPD of the acid catalyts, ACPZr.

To have a further comparison about the Cu active sites activity and how they could be affected by the presence of Zr and P, the turn over frequency (TOF) values for CO conversion, calculated as the $mol_{CO}\ mol_{Cu}^{-1}\ s^{-1}$, were estimated for the catalysts here analyzed, at a temperature of 250 °C. It should be noted that the presence of P species on the carbon surface provided the catalyst with some surface acidity that can promote *in-situ* methanol dehydration, thus, lifting the thermodynamic restrictions of the methanol synthesis process and favoring the CO conversion. Due to the intrinsic nature of the catalytic materials, TOF values comparison could not be made at *iso*-methanol selectivity values, for the same temperature and, thus, these TOF figures should be considered as

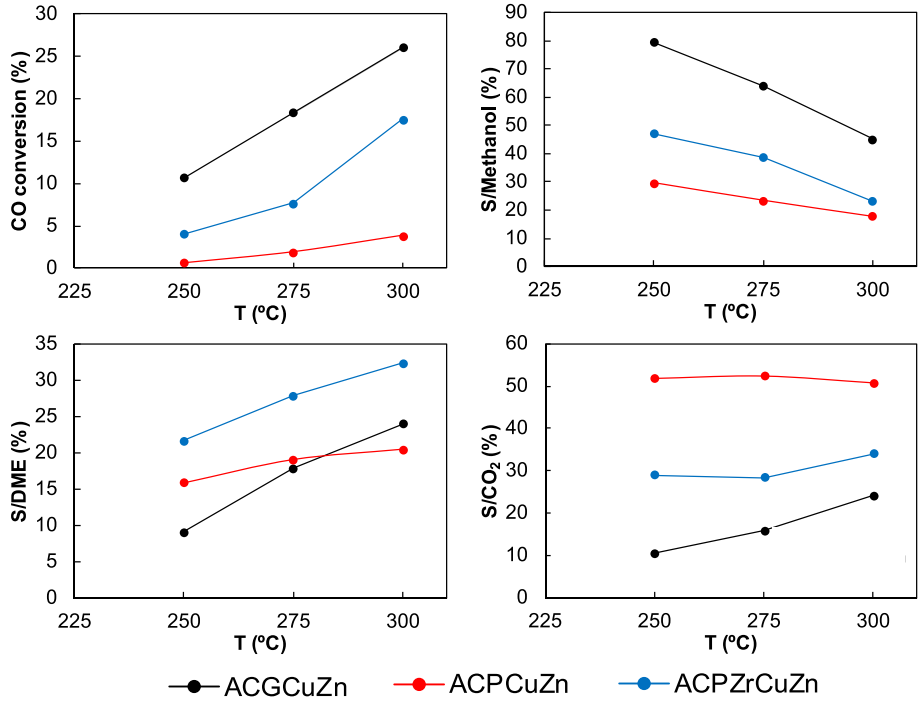

Fig. 6. CO conversion and selectivity to main reaction products (Methanol, DME and CO_2 as function of temperature for the Cu-Zn-loaded activated carbon catalysts ($H_2/CO = 3$, GHSV = 36.4 $L{\cdot}g_{Cu}^{-1}{\cdot}s^{-1}$, 45 bar, 3 h on stream).

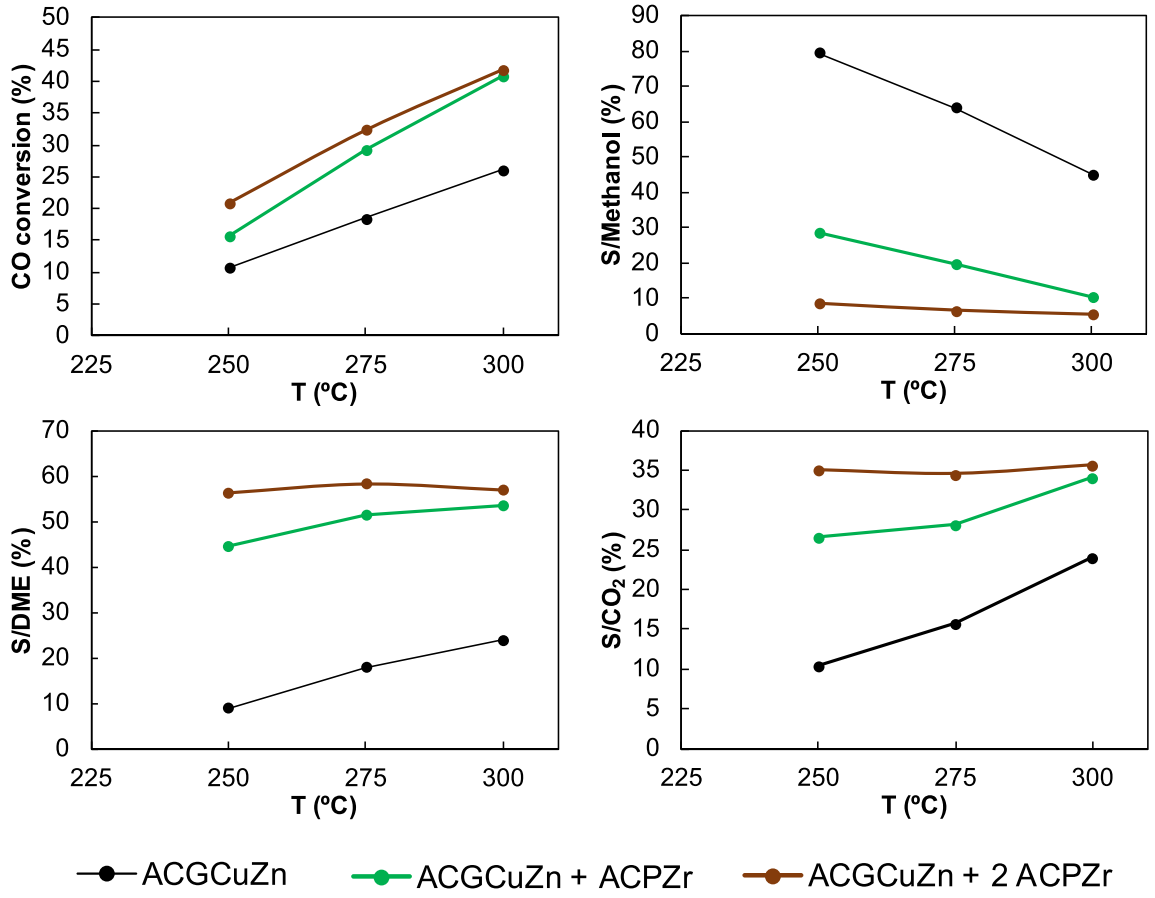

Fig. 7. CO conversion and selectivity to main reaction products (Methanol, DME and CO_2 as function of temperature for the studied Acid/Metallic components mass ratios ($H_2/CO = 3$, GHSV = 36.4 $L{\cdot}g_{Cu}^{-1}{\cdot}s^{-1}$, 45 bar, 3 h on stream).

apparent turn over frequency values. The calculated apparent TOF was $5.6 \bullet 10^{-3}$, $5.1 \bullet 10^{-3}$, and $4.2 \bullet 10^{-3}$ s^{-1}, for *ACGCuZn*, *ACPZrCuZn* and *ACPCuZn*, respectively. These figures indicated slightly higher values with the lower presence (or absence) of copper phosphate species on the catalyst surface, even though a thermodynamic relaxation in the methanol synthesis step, is occurring for these samples presenting acidic character (P-containing samples).

In the light of the catalytic results shown above, despite the higher selectivity to DME value obtained for *ACPZrCuZn*, as compared to the other catalysts here presented, *ACGCuZn* showed the highest methanol and DME yields, with values of 10.8 and 6.3, respectively, and, thus, this catalyst was chosen to be used as methanol synthesis component for the preparation of bifunctional catalytic beds. This was carried out by physically mixing the selected methanol synthesis catalyst (*ACGCuZn*) and the methanol dehydration catalyst (*ACPZr*), by using different mass ratios of the individual catalytic materials. The resulting physical mixtures were used as bifunctional catalytic beds for the direct synthesis of DME from syngas. Fig. 7 presents the CO conversion and selectivity to the main reaction products at different temperatures for the studied catalytic beds (T = 250 – 300 °C, GHSV = 36.4 $L \cdot g_{Cu}^{-1} \cdot s^{-1}$, P = 45 bar, H_2/CO = 3). As commented above, *ACGCuZn* presented a high selectivity to methanol at 250 °C, which dropped when increasing the temperature due to the formation of DME and CO_2. When analyzing catalytic bed prepared keeping an Acid/metallic catalyst mass ratio value of 1, *ACGCuZn + 1 ACPZr*, it could be observed that the carbon-based methanol dehydration catalyst, *ACPZr*, which presents Zr-O-P acid sites with suitable catalytic behavior for the selective methanol dehydration to DME, was capable promoting the methanol dehydration under the syngas to DME reaction conditions, thus achieving a higher selectivity to DME value than the isolated methanol synthesis catalyst, *ACGCuZn*. Moreover, as expected, a higher CO conversion value was obtained due to the synergic effect achieved when integrating both methanol synthesis and dehydration in the same reactor [19,26]. The increase of the acid/metallic catalyst mass ratio to a value of 2, *ACGCuZn + 2 ACPZr*, resulted in a further increase of the dehydration activity of the catalytic bed, achieving a higher CO conversion and selectivity to DME values as compared to the one obtained keeping an acid/metallic catalysts mass ratio of 1, *ACGCuZn + 1 ACPZr*. Analyzing the selectivity to the reaction products obtained for the two acid/metallic catalysts mass ratios studied, it could be observed that the products distribution was affected by the reaction temperature in the case of *ACGCuZn + 1 ACPZr*, showing an increase in the selectivity to DME and CO_2 by increasing the temperature from 250 to 300 °C, where the same CO conversion and product distribution that the obtained for *ACGCuZn + 2 ACPZr* were achieved. Given that methanol dehydration reaction is kinetically faster than methanol synthesis reaction [87], these results suggested that in the case of the use of an acid/metallic catalysts mass ratio of 1, for low temperatures, the overall formation of methanol (methanol production rate) was higher than methanol consumption, through its dehydration. This higher methanol production than consumption rate indicated that the total number of acid sites was not enough, so as to promote methanol dehydration reaction to the maximum attainable extent, at low temperatures, in the case of this catalytic system. On the other hand, when analyzing the catalytic system containing an acid/metallic ratio of 2, *ACGCuZn + 2 ACPZr*, it was observed that the product distribution remained unaltered in the whole temperature range. In this case, methanol consumption rate was higher than methanol production at all operation conditions, indicating that the number of acid sites was in this case sufficient to promote methanol dehydration to the maximum attainable extent, making the overall product distribution kinetically controlled by the methanol synthesis reaction.

These results, clearly highlight that the direct DME synthesis from syngas can be efficiently carried out by exclusively using carbon-based catalysts. In this sense, the metallic function showed a good catalytic behavior for CO hydrogenation and, on the other hand, the acid function exhibited suitable acidic properties for the selective methanol dehydration to DME under the syngas to DME reaction conditions. Regarding stability of the catalysts, only a slow deactivation with time on stream for long operation times, without significantly altering the product distribution, was observed. Although a deep understanding of catalyst deactivation is out of the scope of the present work, this slow decrease in the activity could be related to coke deposition on the metallic sites and/or Cu sintering, which have been reported to be the main responsible phenomena for direct DME synthesis catalysts deactivation [7,88].

When comparing the catalytic beds here presented with other catalytic beds/bifunctional catalysts reported in the literature, it is worth it remarking that the catalysts present in this study were prepared from inexpensive industrial waste. As regarding the CO conversion obtained, it is important to highlight that, in contrast with other inorganic catalysts [17,89], in which the whole material can be considered as an active phase for the chemical reaction involved, only 5 %(w/w) and 16 % (w/w) of the waste-derived material, for the methanol dehydration and methanol synthesis catalysts, respectively, should be considered as an active phase for the reactions involved in the syngas to DME process. Therefore, the space velocity, with respect to the catalytic active phase, used in the present work is considerably higher than that reported for other catalysts. Despite this high active phase-based space velocity, the catalysts reported in the present study, showed a noticeable catalytic activity, making it possible to achieve CO conversion values comparable to that reported for other catalysts [5,24,76,85]. The selectivity to DME values here obtained were also outstanding, with a value of 58.4 % at 275 °C. Several studies can be found in literature dealing with the preparation of inorganic-based catalyst for the direct syngas to DME process, in which selectivity values range from 51 to 63 % [90–92]. A comparison between the carbon-based catalytic system and these inorganic-based catalysts showed that advanced catalytic systems, such as core shell or fibrillary structured catalysts slightly outperform the present carbon-based catalytic system, which could be related to the intimate contact and spatial arrangement of the metallic an acidic function in the catalyst bed [91,92]. However, similar or even higher selectivity values were achieved in the present study when compared to catalytic beds prepared by physically mixing the individual metallic and acid components [90,93,94].

4. Conclusions

The direct DME synthesis from syngas was efficiently achieved by using activated carbon-based catalysts. Two kinds of activated carbons, prepared by physical (by CO_2 partial gasification) and chemical (with phosphoric acid) activation of olive stones, were used as supports for the preparation of the catalysts. The main difference between them was the presence of chemically stable phosphorus surface groups, mainly in form of C-O-PO_3 groups, on the activated carbon prepared via chemical activation with phosphoric acid, which demonstrated to play a critical role on the performance of the catalysts.

As for the methanol dehydration catalyst, a Zr-loaded chemically activated carbon was used. The zirconium phosphate species, present on the carbon surface, exhibited an excellent acid character for the selective methanol dehydration to DME under syngas-to-DME process conditions. For the methanol synthesis component, the two activated carbons and the methanol dehydration catalyst were loaded with Cu-Zn and evaluated. The presence of phosphorus groups on the surface of the activated carbons played a major role on the catalytic performance of the materials. The results showed strong interactions between the metallic phase and the phosphate surface groups, due to the formation Cu phosphate species, which were not active for the methanol synthesis reaction. On the contrary, the physically activated carbon, not containing phosphorus, exhibited a fairly good catalytic behavior.

The preparation of bifunctional catalysts was attempted using the methanol dehydration catalyst as support of the metallic phase. By this way a higher selectivity to DME compared to the rest of the methanol

synthesis catalysts presented here was attained. However, CO conversion was reduced due to the detrimental interaction between Cu and the phosphate species, which made this preparation strategy unfeasible for obtaining relevant DME yields.

On the other hand, the physical mixing of the methanol synthesis and methanol dehydration catalysts resulted in the preparation of carbon-based catalytic beds, which avoided the metallic-acid detrimental interaction. These carbon-based catalytic beds performed very efficiently in the direct DME synthesis from syngas. Different mass ratios of the individual catalysts were studied. An acid/metallic catalyst mass ratio of 2 provided the catalytic bed with enough acid sites for making the overall syngas to DME process kinetically controlled by the methanol synthesis reaction.

CRediT authorship contribution statement

José Palomo: Writing – original draft, Methodology, Investigation, Formal analysis, Data curation, Conceptualization. **Miguel Ángel Rodríguez-Cano:** Methodology, Investigation, Formal analysis, Data curation. **José Rodríguez-Mirasol:** Writing – review & editing, Supervision, Project administration, Funding acquisition, Formal analysis. **Tomás Cordero:** Writing – review & editing, Supervision, Project administration, Funding acquisition, Formal analysis.

Declaration of competing interest

The authors declare that they have no known competing financial interests or personal relationships that could have appeared to influence the work reported in this paper.

Data availability

Data will be made available on request.

Acknowledgements

This work was supported by MCIN (PID2022-140844OB-I00 and TED2021-131324B-C21) and European Union "NextGenerationEU"/PRTR (MCIN/AEI/10.13039/501100011033). Funding for open access charge: Universidad de Malaga / CBUA J. Palomo acknowledges the assistance of the Spanish Ministry Education for the award of FPU grant (FPU13/02413). M. A. Rodríguez-Cano also acknowledges the assistance of the Spanish Ministry of Sciences Innovation and Universities for the concession of a FPU grant (FPU18/02796).

Appendix A. Supplementary material

Supplementary data to this article can be found online at https://doi.org/10.1016/j.fuel.2024.131264.

References

[1] Semelsberger TA, Borup RL, Greene HL. Dimethyl ether (DME) as an alternative fuel. J Power Sources 2006;156:497–511. https://doi.org/10.1016/j.jpowsour.2005.05.082.
[2] Fleisch TH, Basu A, Gradassi MJ, Masin JG. Dimethyl ether: a fuel for the 21st century. Stud Surf Sci Catal 1997;107:117–25. https://doi.org/10.1016/S0167-2991(97)80323-0.
[3] Sorenson SC. Dimethyl ether in diesel engines: progress and perspectives. J Eng Gas Turbines Power 2001;123:652–8. https://doi.org/10.1115/1.1370373.
[4] Arcoumanis C, Bae C, Crookes R, Kinoshita E. The potential of di-methyl ether (DME) as an alternative fuel for compression-ignition engines : a review. Fuel 2008;87:1014–30. https://doi.org/10.1016/j.fuel.2007.06.007.
[5] Saravanan K, Ham H, Tsubaki N, Bae JW. Recent progress for direct synthesis of dimethyl ether from syngas on the heterogeneous bifunctional hybrid catalysts. Appl Catal B Environ 2017;217:494–522. https://doi.org/10.1016/j.apcatb.2017.05.085.
[6] Singh R, Tripathi K, Pant KK, Parikh JK. Unravelling synergetic interaction over tandem Cu-ZnO-ZrO_2/hierarchical ZSM5 catalyst for CO_2 hydrogenation to methanol and DME. Fuel 2022;318:123641. https://doi.org/10.1016/j.fuel.2022.123641.
[7] Ateka A, Rodriguez-Vega P, Ereña J, Aguayo AT, Bilbao J. Kinetic modeling and reactor design of the direct synthesis of dimethyl ether for CO_2 valorization. A review. Fuel 2022;327. doi:10.1016/j.fuel.2022.125148.
[8] Ozcan MC, Karaman BP, Oktar N, Dogu T. Dimethyl ether from syngas and effect of CO_2 sorption on product distribution over a new bifunctional catalyst pair containing STA@SBA-15. Fuel 2022;330:125607. https://doi.org/10.1016/j.fuel.2022.125607.
[9] Liu Z, Sun C, Wang G, Wang Q, Cai G. New progress in R&D of lower olefin synthesis. Fuel Process Technol 2000;62:161–72. https://doi.org/10.1016/S0378-3820(99)00117-4.
[10] Baltes C, Vukojević S, Schüth F. Correlations between synthesis, precursor, and catalyst structure and activity of a large set of CuO/ZnO/Al_2O_3 catalysts for methanol synthesis. J Catal 2008;258:334–44. https://doi.org/10.1016/j.jcat.2008.07.004.
[11] Grunwaldt JD, Molenbroek AM, Topsoe NY, Topsoe H, Clausen BS. In situ investigations of structural changes in Cu/ZnO catalysts. J Catal 2000;194:452–60. https://doi.org/10.1006/jcat.2000.2930.
[12] Chinchen GC, Denny PJ, Jennings JR, Spencer MS, Waugh KC. Synthesis of methanol. part 1. catalysts and kinetics. Appl Catal 1988;36:1–65. https://doi.org/10.1016/S0166-9834(00)80103-7.
[13] Seo CW, Jung KD, Lee KY, Yoo KS. Dehydration of methanol over nordstrandite based catalysts for dimethyl ether synthesis. J Ind Eng Chem 2009;15:649–52. https://doi.org/10.1016/J.JIEC.2009.09.037.
[14] Bercic G, Levec J. Catalytic dehydration of methanol to dimethyl ether. Kinetic investigation and reactor simulation. Ind Eng Chem Res 1993;32:2478–84. https://doi.org/10.1021/ie00023a006.
[15] Yaripour F, Baghaei F, Schmidt I, Perregaard J. Catalytic dehydration of methanol to dimethyl ether (DME) over solid-acid catalysts. Catal Commun 2005;6:147–52. https://doi.org/10.1016/J.CATCOM.2004.11.012.
[16] Xu M, Lunsford JH, Goodman DW, Bhattacharyya A. Synthesis of dimethyl ether (DME) from methanol over solid-acid catalysts. Appl Catal A Gen 1997;149:289–301. https://doi.org/10.1016/S0926-860X(96)00275-X.
[17] Ateka A, Sierra I, Ereña J, Bilbao J, Aguayo AT. Performance of CuO-ZnO-ZrO_2 and CuO-ZnO-MnO as metallic functions and SAPO-18 as acid function of the catalyst for the synthesis of DME CO-feeding CO_2. Fuel Process Technol 2016;152:34–45. https://doi.org/10.1016/j.fuproc.2016.05.041.
[18] Dadgar F, Myrstad R, Pfeifer P, Holmen A, Venvik HJ. Direct dimethyl ether synthesis from synthesis gas: the influence of methanol dehydration on methanol synthesis reaction. Catal Today 2016;270:76–84. https://doi.org/10.1016/j.cattod.2015.09.024.
[19] Aguayo AT, Ereña J, Mier D, Arandes JM, Olazar M, Bilbao J. Kinetic modeling of dimethyl ether synthesis in a single step on a CuO−ZnO−Al_2O_3/γ-Al_2O_3 catalyst. Ind Eng Chem Res 2007;46:5522–30. https://doi.org/10.1021/IE070269S.
[20] García-Trenco A, Martínez A. Direct synthesis of DME from syngas on hybrid CUZNAL/ZSM-5 catalysts: new insights into the role of zeolite acidity. Appl Catal A Gen 2012;411–412:170–9. https://doi.org/10.1016/j.apcata.2011.10.036.
[21] Ereña J, Garoña R, Arandes JM, Aguayo AT, Bilbao J. Effect of operating conditions on the synthesis of dimethyl ether over a CuO-ZnO-Al_2O_3/NaHZSM-5 bifunctional catalyst. Catal Today 2005;107–108:467–73. https://doi.org/10.1016/j.cattod.2005.07.116.
[22] Sun J, Yang G, Yoneyama Y, Tsubaki N. Catalysis chemistry of dimethyl ether synthesis. ACS Catal 2014;4:3346–56. https://doi.org/10.1021/cs500967j.
[23] Banivaheb S, Pitter S, Delgado KH, Rubin M, Sauer J, Dittmeyer R. Recent Progress in direct DME synthesis and potential of bifunctional catalysts. Chem-Ing-Tech 2022;94:240–55. https://doi.org/10.1002/cite.202100167.
[24] Ateka A, Pérez-Uriarte P, Sánchez-Contador M, Ereña J, Aguayo AT, Bilbao J. Direct synthesis of dimethyl ether from syngas on CuO-ZnO-MNO/SAPO-18 bifunctional catalyst. Int J Hydrogen Energy 2016;41:18015–26. https://doi.org/10.1016/j.ijhydene.2016.07.195.
[25] Olah GA, Goeppert A, Prakash GKS. Beyond oil and gas : the methanol economy. Wiley-VCH; 2009.
[26] Shen W-J, Jun K-W, Choi H-S, Lee K-W. Thermodynamic investigation of methanol and dimethyl ether synthesis from CO_2 hydrogenation. Korean J Chem Eng 2000;17:210–6. https://doi.org/10.1007/BF02707145.
[27] Lu W, Teng L, Xiao W. Simulation and experiment study of dimethyl ether synthesis from syngas in a fluidized-bed reactor. Chem Eng Sci 2004;59:5455–64. https://doi.org/10.1016/j.ces.2004.07.031.
[28] Hua Y, Guo X, Mao D, Lu G, Rempel GL, Ng FTT. Single-step synthesis of dimethyl ether from biomass-derived syngas over CuO-ZnO-MOx(M = Zr, Al, Cr, Ti)/HZSM-5 hybrid catalyst: effects of MOx. Appl Catal A Gen 2017;540:68–74. https://doi.org/10.1016/j.apcata.2017.04.015.
[29] Gadek M, Kubica R, Jedrysik E. Production of methanol and dimethyl ether from biomass derived syngas - a comparison of the different synthesis pathways by means of flowsheet simulation. Comput Aided Chem Eng 2013;32:55–60. https://doi.org/10.1016/B978-0-444-63234-0.50010-5.
[30] Wang Z, He T, Li J, Wu J, Qin J, Liu G, et al. Design and operation of a pilot plant for biomass to liquid fuels by integrating gasification, DME synthesis and DME to gasoline. Fuel 2016;186:587–96. https://doi.org/10.1016/j.fuel.2016.08.108.
[31] Giuliano A, Catizzone E, Freda C. Process simulation and environmental aspects of dimethyl ether production from digestate-derived syngas. Int J Environ Res Public Health 2021;18:1–21. https://doi.org/10.3390/ijerph18020807.
[32] Tyagi P, Kumar V. Present and future perspectives of liquid-phase slurry processes involved in methanol and dimethyl ether synthesis using biomass-derived syngas. Energy Fuel 2023;37:3328–54. https://doi.org/10.1021/acs.energyfuels.2c02768.

[33] Gao R, Zhang L, Wang L, Zhang C, Jun KW, Ki Kim S, et al. Conceptual design of full carbon upcycling of CO_2 into clean DME fuel: techno-economic assessment and process optimization. Fuel 2023;344:128120. https://doi.org/10.1016/j.fuel.2023.128120.

[34] Djinović P, Schüth F. Chapter 12 - Energy Carriers Made from Hydrogen. Electrochem. Energy Storage Renew. Sources Grid Balanc., 2015, p. 183–99. doi: 10.1016/B978-0-444-62616-5.00012-7.

[35] Catizzone E, Freda C, Braccio G, Frusteri F, Bonura G. Dimethyl ether as circular hydrogen carrier: catalytic aspects of hydrogenation/dehydrogenation steps. J Energy Chem 2021;58:55–77. https://doi.org/10.1016/j.jechem.2020.09.040.

[36] Pawelczyk E, Łukasik N, Wysocka I, Rogala A, Gębicki J. Recent Progress on hydrogen storage and production using chemical hydrogen carriers. Energies 2022: 15. https://doi.org/10.3390/en15144964.

[37] Guo X, Mao D, Lu G, Wang S, Wu G. Glycine–nitrate combustion synthesis of CuO–ZnO–ZrO_2 catalysts for methanol synthesis from CO_2 hydrogenation. J Catal 2010;271:178–85. https://doi.org/10.1016/J.JCAT.2010.01.009.

[38] Ereña J, Sierra I, Olazar M, Gayubo AG, Aguayo AT. Deactivation of a CuO-ZnO-Al_2O_3/γ-Al_2O_3 catalyst in the synthesis of dimethyl ether. Ind Eng Chem Res 2008; 47:2238–47.

[39] Song X, Yang C, Li X, Wang Z, Pei C, Zhao ZJ, et al. On the role of hydroxyl groups on Cu/Al_2O_3 in CO_2 hydrogenation. ACS Catal 2022;12:14162–72. https://doi.org/10.1021/acscatal.2c03591.

[40] Ge Q, Huang Y, Qiu F, Li S. Bifunctional catalysts for conversion of synthesis gas to dimethyl ether. Appl Catal A Gen 1998;167:23–30.

[41] Palomo J, Rodríguez-Cano MA, Berruezo-García J, Rodríguez-Mirasol J, Cordero T. Efficient methanol dehydration to DME and light hydrocarbons by submicrometric ZrO_2-ZSM-5 fibrillar catalysts with a shell-like structure. Fuel 2022:315. https://doi.org/10.1016/j.fuel.2022.123283.

[42] Xia J, Mao D, Tao W, Chen Q, Zhang Y, Tang Y. Dealumination of HMCM-22 by various methods and its application in one-step synthesis of dimethyl ether from syngas. Microporous Mesoporous Mater 2006;91:33–9. https://doi.org/10.1016/J.MICROMESO.2005.11.014.

[43] Bonura G, Cannilla C, Frusteri L, Mezzapica A, Frusteri F. DME production by CO_2 hydrogenation: key factors affecting the behaviour of CuZnZr/ferrierite catalysts. Catal Today 2017;281:337–44. https://doi.org/10.1016/J.CATTOD.2016.05.057.

[44] Jung HS, Zafar F, Wang X, Nguyen TX, Hong CH, Hur YG, et al. Morphology effects of ferrierite on bifunctional cu-ZnO-Al_2O_3/Ferrierite for direct syngas conversion to dimethyl ether. ACS Catal 2021;11:14210–23. https://doi.org/10.1021/acscatal.1c04451.

[45] Du C, Hondo E, Gapu Chizema L, Hassan Ali R, Chang X, Dai L, et al. An efficient microcapsule catalyst for one-step ethanol synthesis from dimethyl ether and syngas. Fuel 2021;283:1–10. https://doi.org/10.1016/j.fuel.2020.118971.

[46] Cotoruelo LM, Marqués MD, Díaz FJ, Rodríguez-Mirasol J, Rodríguez JJ, Cordero T. Equilibrium and kinetic study of Congo red adsorption onto lignin-based activated carbons. Transp Porous Media 2010;83:573–90. https://doi.org/10.1007/s11242-009-9460-8.

[47] Rosas JM, Bedia J, Cordero T. On the preparation and characterization of chars and activated carbons from orange skin. Fuel Process Technol 2010;91:1345–54. https://doi.org/10.1016/j.fuproc.2010.05.006.

[48] Robinson WRAM, Mol JC. Support effects in methanol synthesis over copper-containing catalysts. Appl Catal 1991;76:117–29. https://doi.org/10.1016/0166-9834(91)80008-K.

[49] Iranmahboob J, Hill DO. Alcohol synthesis from syngas over K_2CO_3/CoS/MoS_2 on activated carbon. Catal Letters 2002;78:49–55. https://doi.org/10.1023/A:1014945032402.

[50] Duan H, Yang Y, Patel J, Burke N, Zhai Y, Webley PA, et al. The effect of the modification methods on the catalytic performance of activated carbon supported CuO-ZnO catalysts. Carbon Lett 2018;25:33–42. https://doi.org/10.5714/CL.2018.25.033.

[51] Van Den Berg R, Prieto G, Korpershoek G, Van Der Wal LI, Van Bunningen AJ, Lægsgaard-Jørgensen S, et al. Structure sensitivity of Cu and CuZn catalysts relevant to industrial methanol synthesis. Nat Commun 2016:7. https://doi.org/10.1038/ncomms13057.

[52] Zawadzki J, Wiśniewski M, Weber J, Heintz O, Azambre B. IR study of adsorption and decomposition of propan-2-ol on carbon and carbon-supported catalysts. Carbon 2001;39:187–92. https://doi.org/10.1016/S0008-6223(00)00107-X.

[53] Jasińska J, Krzyżyńska B, Kozłowski M. Influence of activated carbon modifications on their catalytic activity in methanol and ethanol conversion reactions. Cent Eur J Chem 2011;9:925–31. https://doi.org/10.2478/s11532-011-0078-7.

[54] Moreno-Castilla C, Carrasco-Marín F, Parejo-Pérez C, López Ramón MV. Dehydration of methanol to dimethyl ether catalyzed by oxidized activated carbons with varying surface acidic character. Carbon 2001;39:869–75. https://doi.org/10.1016/S0008-6223(00)00192-5.

[55] Valero-Romero MJ, García-Mateos FJ, Rodríguez-Mirasol J, Cordero T. Role of surface phosphorus complexes on the oxidation of porous carbons. Fuel Process Technol 2017;157:116–26. https://doi.org/10.1016/J.FUPROC.2016.11.014.

[56] Bedia J, Barrionuevo R, Rodríguez-Mirasol J, Cordero T. Ethanol dehydration to ethylene on acid carbon catalysts. Appl Catal B Environ 2011;103:302–10. https://doi.org/10.1016/J.APCATB.2011.01.032.

[57] Bedia J, Ruiz-Rosas R, Rodríguez-Mirasol J, Cordero T. Kinetic study of the decomposition of 2-butanol on carbon-based acid catalyst. AIChE J 2010;56: 1557–68. https://doi.org/10.1002/aic.12056.

[58] Valero Romero MJ, Calvo Muñoz EM, Ruíz Rosas R, Rodríguez-Mirasol J, Cordero T. Phosphorus-containing mesoporous carbon acid catalyst for methanol dehydration to dimethyl ether. Ind Eng Chem Res 2019;58:4042–53. https://doi.org/10.1021/acs.iecr.8b05897.

[59] Palomo J, Rodríguez-Mirasol J, Cordero T. Methanol dehydration to dimethyl ether on Zr-loaded P-containing mesoporous activated carbon catalysts. Materials (Basel) 2019:12. https://doi.org/10.3390/ma12132204.

[60] Palomo J, Rodríguez-Cano MA, Rodríguez-Mirasol J, Cordero T. On the kinetics of methanol dehydration to dimethyl ether on zr-loaded P-containing mesoporous activated carbon catalyst. Chem Eng J 2019:378. https://doi.org/10.1016/j.cej.2019.122198.

[61] Goda MN, Abdelhamid HN, Said AEAA. Zirconium oxide sulfate-carbon (ZrOSO4@C) derived from carbonized UiO-66 for selective production of dimethyl ether. ACS Appl Mater Interfaces 2020;12:646–53. https://doi.org/10.1021/acsami.9b17520.

[62] Khalil KMS, Elhamdy WA, Goda MN, Said AEAA. Biomass derived P-containing activated carbon as a novel green catalyst/support for methanol conversion to dimethyl ether alternative fuel. J Environ Chem Eng 2021;9:106572. https://doi.org/10.1016/j.jece.2021.106572.

[63] Brunauer S, Emmett PH, Teller E. Adsorption of gases in multimolecular layers. J Am Chem Soc 1938;60:309–19. https://doi.org/10.1021/ja01269a023.

[64] Lowell S, Shields JE, Morral JE. Powder Surface Area and Porosity, 2nd Edition. vol. 107. 1985. doi:10.1115/1.3225796.

[65] Dubinin MM. The potential theory of adsorption of gases and vapors for adsorbents with energetically nonuniform surfaces. Chem Rev 1960;60:235–41. https://doi.org/10.1021/cr60204a006.

[66] Biniak S, Szymansky G, Siedlewski J, Swiatkowski A. The characterization of activated carbons with oxygen and nitrogen surface groups. Carbon 1997;35: 1799–810. https://doi.org/10.1016/S0008-6223(97)00096-1.

[67] Desimoni E, Casella GI, Morone A, Salvi AM. XPS determination of oxygen-containing functional groups on carbon-fibre surfaces and the cleaning of these surfaces. Surf Interface Anal 1990;15:627–34. https://doi.org/10.1002/sia.740151011.

[68] Thommes M, Kaneko K, Neimark A V., Olivier JP, Rodriguez-Reinoso F, Rouquerol J, et al. Physisorption of gases, with special reference to the evaluation of surface area and pore size distribution (IUPAC Technical Report). vol. 87. 2015. doi: 10.1515/pac-2014-1117.

[69] Jagtoyen M, Derbyshire F. Activated carbons from yellow poplar and white oak by H3PO4activation. Carbon 1998;36:1085–97. https://doi.org/10.1016/S0008-6223(98)00082-7.

[70] Rosas JM, Bedia J, Rodríguez-Mirasol J, Cordero T. HEMP-derived activated carbon fibers by chemical activation with phosphoric acid. Fuel 2009;88:19–26. https://doi.org/10.1016/j.fuel.2008.08.004.

[71] Molina-Sabio M, Pérez V, Rodríguez-Reinoso F. Impregnation of activated carbon with chromium and copper salts: effect of porosity and metal content. Carbon 1994;32:1259–65. https://doi.org/10.1016/0008-6223(94)90111-2.

[72] Bedia J, Rosas JM, Márquez J, Rodríguez-Mirasol J, Cordero T. Preparation and characterization of carbon based acid catalysts for the dehydration of 2-propanol. Carbon 2009;47:286–94. https://doi.org/10.1016/j.carbon.2008.10.008.

[73] Alberti G, Costantino U, Marletta G, Puglisi O, Pignataro S. ESCA investigations of amorphous and crystalline zirconium acid phosphates. J Inorg Nucl Chem 1981;43: 3329–34. https://doi.org/10.1016/0022-1902(81)80111-X.

[74] Colón JL, Thakur DS, Yang CY, Clearfield A, Martini CR. X-ray photoelectron spectroscopy and catalytic activity of α-zirconium phosphate and zirconium phosphate sulfophenylphosphonate. J Catal 1990;124:148–59. https://doi.org/10.1016/0021-9517(90)90111-V.

[75] Simón E, Rosas JM, Santos A, Romero A. Study of the deactivation of copper-based catalysts for dehydrogenation of cyclohexanol to cyclohexanone. Catal Today 2012;187:150–8. https://doi.org/10.1016/j.cattod.2011.10.010.

[76] Bae JW, Kang S-H, Lee Y-J, Jun K-W. Synthesis of DME from syngas on the bifunctional Cu–ZnO–Al_2O_3/Zr-modified ferrierite: effect of Zr content. Appl Catal B Environ 2009;90:426–35. https://doi.org/10.1016/J.APCATB.2009.04.002.

[77] Khattak GD, Salim MA, Hallak AB, Daous MA, Khawaja EE, Wenger LE, et al. Study of valence states of copper in copper-phosphate glasses. J Mater Sci 1995;30: 4032–6. https://doi.org/10.1007/BF00360705.

[78] Salim MA, Khattak GD, Hussain MS. X-ray photoelectron spectroscopy, fourier transform infrared spectroscopy and electrical conductivity studies of copper phosphate glasses. J Non Cryst Solids 1995;185:101–8. https://doi.org/10.1016/0022-3093(94)00683-0.

[79] Avgouropoulos G, Ioannides T, Matralis H. Influence of the preparation method on the performance of CuO–CeO_2 catalysts for the selective oxidation of CO. Appl Catal B Environ 2005;56:87–93. https://doi.org/10.1016/J.APCATB.2004.07.017.

[80] Liu C, Guo X, Guo Q, Mao D, Yu J, Lu G. Methanol synthesis from CO_2 hydrogenation over copper catalysts supported on MgO-modified TiO_2. J Mol Catal A Chem 2016;425:86–93. https://doi.org/10.1016/J.MOLCATA.2016.09.032.

[81] Moradi GR, Nosrati S, Yaripor F. Effect of the hybrid catalysts preparation method upon direct synthesis of dimethyl ether from synthesis gas. Catal Commun 2007;8: 598–606. https://doi.org/10.1016/J.CATCOM.2006.08.023.

[82] Baek S-C, Kang S-H, Bae JW, Lee Y-J, Lee D-H, Lee K-Y. Effect of copper precursors to the activity for dimethyl ether synthesis from syngas over Cu-ZnO/γ-Al_2O_3 bifunctional catalysts. Energy Fuel 2011;25:2438–43. https://doi.org/10.1021/ef200504p.

[83] Asthana S, Samanta C, Bhaumik A, Banerjee B, Voolapalli RK, Saha B. Direct synthesis of dimethyl ether from syngas over Cu-based catalysts: enhanced selectivity in the presence of MgO. J Catal 2016;334:89–101. https://doi.org/10.1016/J.JCAT.2015.10.020.

[84] Vishwanathan V, Jun KW, Kim JW, Roh HS. Vapour phase dehydration of crude methanol to dimethyl ether over na-modified H-ZSM-5 catalysts. Appl Catal A Gen 2004;276:251–5. https://doi.org/10.1016/j.apcata.2004.08.011.

[85] Phan XK, Bakhtiary HD, Myrstad R, Thormann J, Pfeifer P, Venvik HJ, et al. Preparation and performance of a catalyst-coated stacked foil microreactor for the

methanol synthesis. Ind Eng Chem Res 2010;49:10934–41. https://doi.org/10.1021/ie1005405.
[86] Phan XK, Bakhtiary-Davijany H, Myrstad R, Pfeifer P, Venvik HJ, Holmen A. Preparation and performance of Cu-based monoliths for methanol synthesis. Appl Catal A Gen 2011;405:1–7. https://doi.org/10.1016/j.apcata.2011.07.005.
[87] García-Trenco A, Valencia S, Martínez A. The impact of zeolite pore structure on the catalytic behavior of CuZnAl/zeolite hybrid catalysts for the direct DME synthesis. Appl Catal A Gen 2013;468:102–11. https://doi.org/10.1016/J.APCATA.2013.08.038.
[88] Sierra I, Ereña J, Aguayo AT, Arandes JM, Olazar M, Bilbao J. Co-feeding water to attenuate deactivation of the catalyst metallic function (CuO-ZnO-Al2O3) by coke in the direct synthesis of dimethyl ether. Appl Catal B Environ 2011;106:167–73. https://doi.org/10.1016/j.apcatb.2011.05.021.
[89] Prasad PSS, Bae JW, Kang S, Lee Y, Jun K. Single-step synthesis of DME from syngas on Cu – ZnO – Al2O3/zeolite bifunctional catalysts: the superiority of ferrierite over the other zeolites. Fuel Process Technol 2008;89:1281–6. https://doi.org/10.1016/j.fuproc.2008.07.014.
[90] Khoshbin R, Haghighi M. Direct syngas to DME as a clean fuel: the beneficial use of ultrasound for the preparation of CuO-ZnO-Al_2O_3/HZSM-5 nanocatalyst. Chem Eng Res Des 2013;91:1111–22. https://doi.org/10.1016/j.cherd.2012.11.017.
[91] Wang Y, Wang W, Chen Y, Ma J, Li R. Synthesis of dimethyl ether from syngas over core-shell structure catalyst CuO-ZnO-Al_2O_3@SiO_2-Al_2O_3. Chem Eng J 2014;250:248–56. https://doi.org/10.1016/j.cej.2014.04.018.
[92] Palomo J, Rodríguez-Cano MÁ, Rodríguez-Mirasol J, Cordero T. ZSM-5-decorated CuO/ZnO/ZrO_2 fibers as efficient bifunctional catalysts for the direct synthesis of DME from syngas. Appl Catal B Environ 2020;270. doi:10.1016/j.apcatb.2020.118893.
[93] Khoshbin R, Haghighi M, Asgari N. Direct synthesis of dimethyl ether on the admixed nanocatalystsof CuO-ZnO-Al_2O_3 and HNO_3-modified clinoptilolite at high pressures: surface properties and catalytic performance. Mater Res Bull 2013;48:767–77. https://doi.org/10.1016/j.materresbull.2012.11.057.
[94] Mao D, Yang W, Xia J, Zhang B, Song Q, Chen Q. Highly effective hybrid catalyst for the direct synthesis of dimethyl ether from syngas with magnesium oxide-modified HZSM-5 as a dehydration component. J Catal 2005;230:140–9. https://doi.org/10.1016/j.jcat.2004.12.007.